ENVIRONMENTAL RESEARCH
LETTERS

LETTER • OPEN ACCESS

Effects of anthropogenic heat due to air-conditioning systems on an extreme high temperature event in Hong Kong

To cite this article: Y Wang *et al* 2018 *Environ. Res. Lett.* **13** 034015

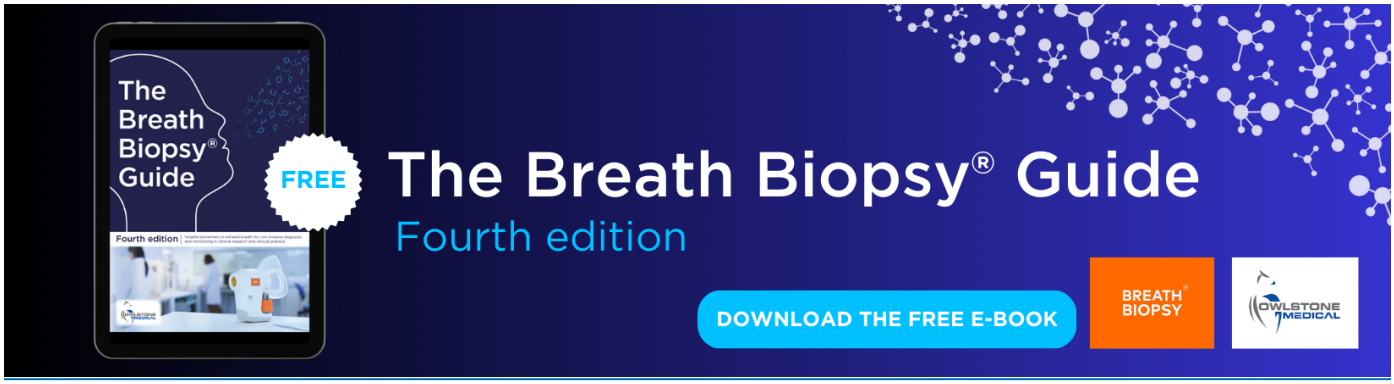

Environmental Research Letters

LETTER

Effects of anthropogenic heat due to air-conditioning systems on an extreme high temperature event in Hong Kong

Y Wang[1,5], Y Li[1], S Di Sabatino[2], A Martilli[3] and P W Chan[4]

1 Department of Mechanical Engineering, The University of Hong Kong, Pokfulam Road, Hong Kong SAR, People's Republic of China
2 Department of Physics and Astronomy Alma Mater Studiorum, University of Bologna, Italy
3 Centro de Investigaciones Energéticas, Medioambientales y Tecnológicas, Madrid, Spain
4 Hong Kong Observatory, Hong Kong SAR, People's Republic of China
5 Author to whom any correspondence should be addressed.

E-mail: wangyi27@connect.hku.hk

OPEN ACCESS

RECEIVED
5 September 2017

REVISED
4 January 2018

ACCEPTED FOR PUBLICATION
17 January 2018

PUBLISHED
22 February 2018

Keywords: anthropogenic heat, air-conditioning systems, direct cooling system, central piped cooling towers, urban heat island circulation, extreme high temperature events, energy consumption

Supplementary material for this article is available online

Abstract

Anthropogenic heat flux is the heat generated by human activities in the urban canopy layer, which is considered the main contributor to the urban heat island (UHI). The UHI can in turn increase the use and energy consumption of air-conditioning systems. In this study, two effective methods for water-cooling air-conditioning systems in non-domestic areas, including the direct cooling system and central piped cooling towers (CPCTs), are physically based, parameterized, and implemented in a weather research and forecasting model at the city scale of Hong Kong. An extreme high temperature event (June 23–28, 2016) in the urban areas was examined, and we assessed the effects on the surface thermal environment, the interaction of sea–land breeze circulation and urban heat island circulation, boundary layer dynamics, and a possible reduction of energy consumption. The results showed that both water-cooled air-conditioning systems could reduce the 2 m air temperature by around 0.5 °C–0.8 °C during the daytime, and around 1.5 °C around 7:00–8:00 pm when the planetary boundary layer (PBL) height was confined to a few hundred meters. The CPCT contributed around 80%–90% latent heat flux and significantly increased the water vapor mixing ratio in the atmosphere by around 0.29 g kg^{-1} on average. The implementation of the two alternative air-conditioning systems could modify the heat and momentum of turbulence, which inhibited the evolution of the PBL height (a reduction of 100–150 m), reduced the vertical mixing, presented lower horizontal wind speed and buoyant production of turbulent kinetic energy, and reduced the strength of sea breeze and UHI circulation, which in turn affected the removal of air pollutants. Moreover, the two alternative air-conditioning systems could significantly reduce the energy consumption by around 30% during extreme high temperature events. The results of this study suggest potential UHI mitigation strategies and can be extended to other megacities to enable them to be more resilient to UHI effects.

Nomenclature

COP	Coefficient of performance [−]
C_p	Specific heat of air [J K^{-1} kg^{-1}]
C_w	Specific heat of water at constant pressure [J K^{-1} kg^{-1}]
C_{sw}	Specific heat of sea water at constant pressure [J K^{-1} kg^{-1}]
d_{ai}	Water vapor mixing ratio of the inlet air [g kg^{-1}]
d_{ao}	Water vapor mixing ratio of the outlet air [g kg^{-1}]
e	Water vapor pressure [hPa]
h_{ai}	Enthalpy of the inlet air [J kg^{-1}]
h_{ao}	Enthalpy of the outlet air [J kg^{-1}]
H_i^{out}	Sensible heat fluxes at each vertical level [W]

H_i Sensible heat generated at each vertical level [W]
H_T^{BASE} Sensible heat generated by Baseline case at rooftop in non-domestic area [W]
H_B^{DCS} Sensible heat generated by DCS case in non-domestic area [W]
H_T^{CPCT} Sensible heat generated by CPCT case in non-domestic area [W]
LE_i^{out} Latent heat fluxes at each vertical level [W]
LE_i Latent heat generated at each vertical level [W]
LE_T^{Base} Latent heat generated by Baseline case at rooftop in non-domestic area [W]
LE_B^{DCS} Latent heat generated by DCS case in non-domestic area [W]
LE_T^{CPCT} Latent heat generated by CPCT case in non-domestic area [W]
L Latent heat of vaporization [J kg^{-1}]
m_a Mass flow rate of the air [kg s^{-1}]
P Atmospheric pressure [hPa]
q_a Air volume flow rate [m^3 s^{-1}]
q_w Water volume flow rate [m^3 s^{-1}]
q_{sw} Sea water volume flow rate [m^3 s^{-1}]
T_{ai} Inlet air temperature [K]
T_{ao} Outlet air temperature [K]
ΔT_w Water temperature difference between inlet and outlet of the condenser [K]
ΔT_{sw} Sea water temperature difference in the condenser in DCS case [K]
Greek Symbols
ν Ratio of the water flow rate and the air flow rate
ρ_a Air density [kg m^{-3}]
ρ_w Water density [kg m^{-3}]
ρ_{sw} Sea water density [kg m^{-3}]
ξ_{CPCT} Heat exchange effectiveness [−]

1. Introduction

The substitution of natural surfaces with impervious urban structures because of rapid ongoing urbanization and human activities has resulted in changes in the urban surface energy and water balance, and has influenced the local atmospheric boundary layer structure and urban climate (Oke 1976, 1988, Bonacquisti *et al* 2006). Almost all the energy consumption for human activities can eventually transform into anthropogenic heat and be released into the atmosphere within the Earth's land–atmosphere system (Taha 1997, Flanner 2009, Xie *et al* 2016). Anthropogenic heat fluxes can increase turbulence fluxes, including both sensible and the latent heat fluxes (Oke 1988). Moreover, anthropogenic heat fluxes influence surface meteorological conditions, particularly air temperature and water vapor pressure; the vertical motion of urban air flow, which in turn affects urban heat island circulation (UHIC) and dynamics and thermal dynamics of the boundary layer; and air pollutants within the urban canopy layer (Oke 1987, 1988, Ichinose *et al* 1999, Kikegawa *et al* 2003, Sailor and Lu 2004, Feng *et al* 2012, Salamanca *et al* 2014, Xie *et al* 2016, Ma *et al* 2017).

Buildings are found to be the major source of anthropogenic heat fluxes; residential and commercial buildings account for 40% of total energy consumption (EIA 2012, Quah and Roth 2012). In the global-scale urban consumption of energy model, heat release from buildings is the largest contributor (89%–96%) of heat emission globally (Allen *et al* 2011). The energy consumption of buildings is likely to increase (Mansur *et al* 2008). Studies on the effects of air-conditioning systems on the urban climate were only found for the cities of Houston, Wuhan, Tokyo, Madrid, and Paris (Ohashi *et al* 2007, Wen and Lian 2009, Salamanca *et al* 2011, 2012, de Munck *et al* 2013). These studies focused mainly on the effect of air-conditioning systems on the outdoor air temperature by using models with different levels of sophistication, did not directly parameterize air-conditioning systems into urban canopy models and neglected the effects of the main physically-based processes on the atmosphere. Wen and Lian (2009) revealed that the domestic use of air conditioners increases the mean air temperature by 0.2 °C or 2.56 °C under neutral and inversion conditions, respectively. Further, de Munck *et al* (2013) found that the temperature increase reached 0.5 °C and 2 °C due to the current and double waste heat release into the atmosphere, respectively. However, the simplified model failed to capture the effects of sensible and latent heat fluxes within the urban canopy layer. Estimation of anthropogenic sensible and latent heat fluxes is difficult, and indirect measurement, empirical estimation, and numerical models are mostly used for this (Grimmond 1992, Kikegawa *et al* 2003, Sailor and Lu 2004, Pigeon *et al* 2007, Salamanca *et al* 2010, Yang *et al* 2014).

The city of Hong Kong is within a humid subtropical climate according to Köppen classification. Electricity consumption in non-domestic buildings accounted for 61.8% of total consumption in June 2016 (www.censtatd.gov.hk). Statistical analysis shows that air-conditioning accounts for around 30% of total electricity consumption, of which 68% is in non-domestic premises (Ho *et al* 2007). The Hong Kong government encourages the adoption of water-cooled air-conditioning systems, including direct cooling systems (DCS) and central piped cooling towers (CPCT), which seems to be an effective method of territory-wide energy improvement and reduction of electricity consumption and greenhouse gas emissions from 2020 onward (Ho *et al* 2007). The effects of the altered air-conditioning systems on the urban thermal and dynamic environment at the city scale are rarely studied but essential. A central component of our study is whether the implementation of two alternative air-conditioning systems can result in an improvement of urban resilience to UHI effects.

Extreme high temperature events and abnormally hot periods are among the most significant climatic stressors for public health, ecosystems, economies, societies, energy consumption, UHI threat, and more (De Bono *et al* 2004, Sharma *et al* 2016, Zampieri *et al* 2016). June 2016 had the second highest temperature in Hong Kong since 1884 (www.weather.gov.hk/) and was the warmest June on record (SCMP, www.scmp.com/tech/science-research/article/1992366/june-2016-warmest-month-record-globally). Therefore, such situations could represent the worst conditions for cooling-energy consumption.

To help overcome the aforementioned gaps in research on the influence of water-cooled air-conditioning systems on climate, in this study, we assess the potential effects of DCS and CPCT systems on an urban scale. Changes in urban air temperature, moisture level, energy fluxes, urban boundary layer structure, local circulations, and potential energy consumption improvement are assessed. Although the results of this study are location dependent, the effectiveness of alternative systems is expected to make other urbanized areas more resilient.

2. Methodology

2.1. Overview of the model

The mesoscale meteorological model has been used to study various meteorological phenomena. The advanced research weather research and forecasting (WRF) model (ARW version 3.6.1) is a non-hydrostatic, compressible model with a mass coordinate system (Skamarock *et al* 2008). The model was set up with four nested domains with 79×79, 79×79, 118×118 and 142×136 grid points possessing spatial resolutions of 13.5, 4.5, 1.5 and 0.5 km, respectively (figure 1(*a*)). The innermost domain covered Hong Kong entirely (figure 1) and provided sufficient information on UHI effects and sea–land breeze circulation (SLBC). The vertical grid contains 51 terrains following full sigma levels from the ground up to 50 hPa. The planetary boundary layer (PBL) scheme of Bougeault and Lacarrere (1989) was used. The other physical schemes used in this study were the single-moment three-class microphysics scheme (Hong *et al* 2004), Dudhia shortwave radiation (Dudhia 1989), RRTM long-wave radiation (Mlawer *et al* 1997), the Noah land surface model (Chen and Dudhia 2001), and Kain–Fritsch (Kain and Fritsch 1990) cumulus schemes for the two outer domains. A 120 h simulation (from 0000 UTC June 23 to 0000 UTC June 28, 2016) was conducted with the initial and boundary conditions from the National Centers for Environmental Prediction (NCEP) Global Forecast System Final Analyses data (FNL) at 1° at 6 h intervals and daily updated sea surface temperatures from NCEP Marine Modeling and Analysis Branch data at 0.5°.

Hong Kong has a large spatial and vertical land surface heterogeneity (figure 1(*b*)). To better represent the dynamics and thermal interacts in the urban canopy layers, multilayer building effect parameterization (BEP, Martilli *et al* 2002) and the building energy model (BEM, Salamanca *et al* 2010) were chosen. The multilayer canopy model, BEP/BEM, with a revised drag coefficient, based on plan area fraction, λ_p, has been tested over Kowloon Peninsula in Hong Kong, and has shown reasonably good results for capturing spatial air temperature distribution, diurnal wind rotation, and stagnation wind phenomena in the lower level convergence zone due to the combination of urban heat island circulation and sea-land breeze circulation (Wang *et al* 2017). The latest gridded building information and land cover and land use data (figure 1(*c*)) were used for the entire Hong Kong area for better representation of spatial heterogeneity. The default air-conditioning system in BEM is the wall-type scenario (shown in figure 2) in all urban areas. In this study the wall-type air-conditioning system is assumed to be used only in residential areas and central air-cooled air systems in non-domestic areas according to the real situation in Hong Kong (shown in figure 2). To study the effect of air-conditioning systems in non-domestic areas on the urban climate in the city of Hong Kong, several configurations or scenarios of air-conditioning systems (shown in figure 2) in non-domestic areas were simulated, as summarized in table 1.

2.2. Air-conditioning systems formulation

The new cooling tower scheme (CPCT case) coupled with the building energy model (BEM) is illustrated. In the counter-flow cooling tower system, the gas phase (cool air) flows upwards and the liquid phase (water) downwards (figure 2) and a large interface exists between the two phases (Milosavljevic and Heikkilä 2001). Heat and mass transfer takes place in the cooling tower system, and the water droplets carry out evaporative cooling with the dry and cool air from the atmosphere (Gutiérrez *et al* 2015). After the process, the water temperature decreases, but the air increases both the temperature and humidity and is released into the atmosphere; further, make-up water is needed for the cooling tower system to maintain the process.

The heat exchange effectiveness, ξ_{CPCT}, between the refrigerant and the water in the condenser is the heat that is generated inside a building at each floor, H_i, which is calculated via the BEM model, and the heat that is pumped into the cooling tower system, H_T^{CPCT}. Assume that no heat is lost in the pipe between the condenser and the cooling tower. Then, the heat exchange effectiveness, ξ_{CPCT}, can be defined as follows:

$$\xi_{\mathrm{CPCT}} = \frac{\sum_{i=1}^{m} H_i}{H_T^{\mathrm{CPCT}}} \tag{1}$$

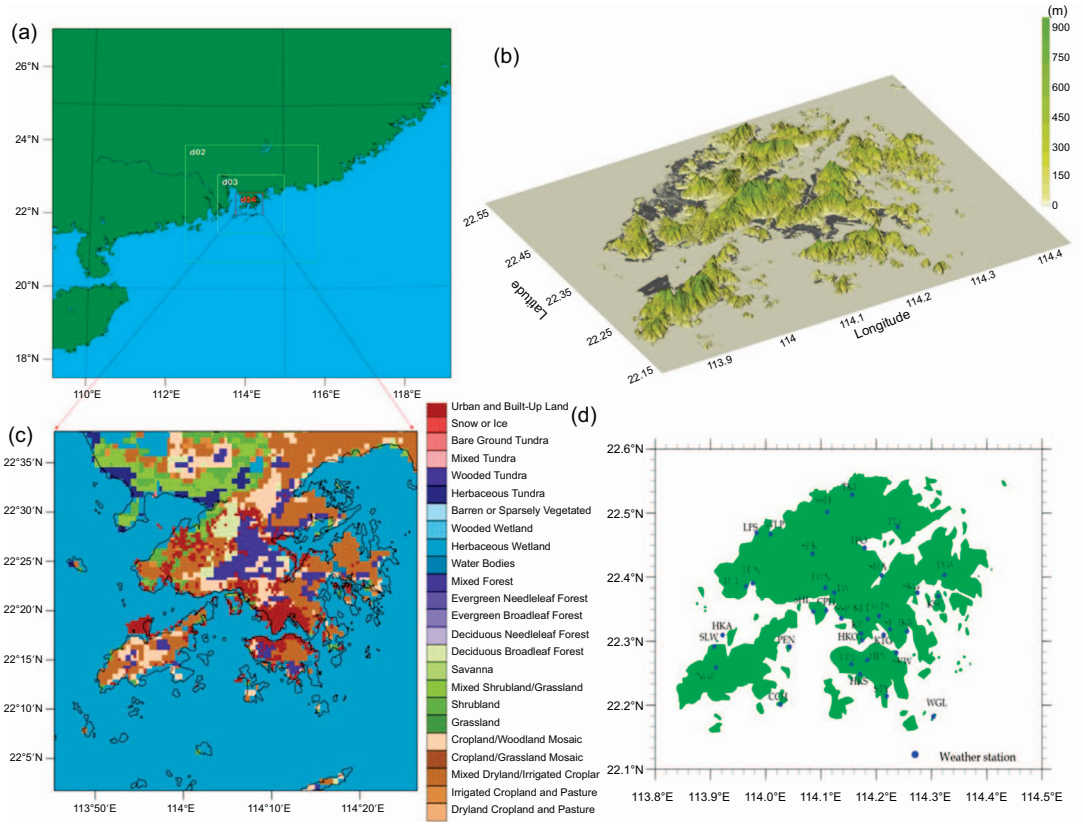

Figure 1. (*a*) WRF modelling domain; (*b*) topography of Hong Kong; (*c*) land cover and land use for the innermost domain with grid resolution of 0.5 km; (*d*) location of weather stations.

Table 1. Configurations and scenarios of air-conditioning systems in non-domestic areas.

Numerical simulations	Urban scheme	Anthropogenic heat release description
Baseline case	BEP/BEM	Based on the real situation, central air-cooled air systems located on the rooftop are used to replace the default wall type air-conditiong systems in BEM (figure 2).
DCS case	BEP/BEM	Direct cooling systems with the use of sea water to cool the condenser located in the buildings is assumed (figure 2).
CPCT case	BEP/BEM	Central piped cooling tower systems are used and assumed to be settled on the rooftop level (figure 2).
No-heat case	BEP/BEM	A scenario without air-conditioning anthropogenic heat releases.

where m represents the total number of floors in the building.

If we assume that the water temperature difference between the inlet and the outlet of the condenser system is constant, then the water volume flow rate is as follows:

$$q_w = \frac{H_T^{\mathrm{CPCT}}}{\rho_w C_w \Delta T_w} \tag{2}$$

where ρ_w denotes the water density, C_w represents the water heat capacity, and ΔT_w stands for the water temperature difference between the inlet and the outlet of the condenser and the cooling tower.

In the counter-flow cooling tower system, the air volume flow rate, q_a, is as follows:

$$q_a = \frac{v q_w \rho_w}{\rho_a} \tag{3}$$

where v denotes the ratio of the water mass flow rate and the air flow rate in the contour-flow cooling tower system, which is determined by the inter-facial contact area and the heat-transfer coefficient, and ρ_w represents the air density. Here, assume that the ratio v is 0.7 (Chen *et al* 2014).

Then, the mass flow rate of the air in the cooling tower system is defined as follows:

$$m_a = \rho_a q_a. \tag{4}$$

The inlet air in the cooling tower is assumed to be from the atmosphere at the appropriate building height level; thus, the enthalpy of the outlet air, h_{ao}, from the cooling tower system can be defined as follows:

$$h_{\mathrm{ao}} = \frac{H_T^{\mathrm{CPCT}}}{m_a} + h_{\mathrm{ai}} \tag{5}$$

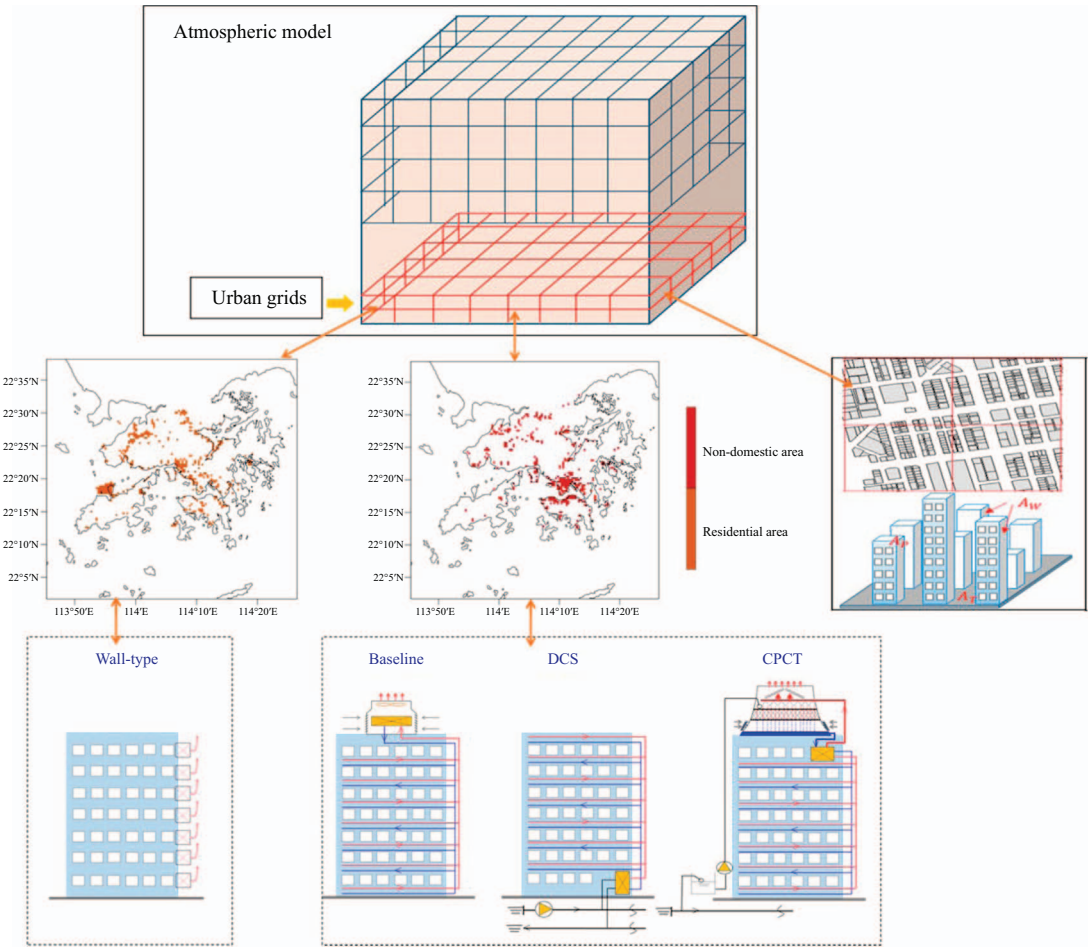

Figure 2. General methodology with wall-type air-conditioning in the residential areas, and Baseline, DCS, and CPCT air-conditioning systems in the non-domestic areas.

where h_{ai} denotes the enthalpy of the inlet air and can be defined as follows:

$$h_{ai} = C_p T_{ai} + d_{ai}\left(C_{pw} + L\right) \tag{6}$$

where C_p denotes the specific heat of air at constant pressure, C_{pw} represents the specific heat of water at constant pressure, L indicates the latent heat of vaporization, and T_{ai} and d_{ai} refer to the air temperature and the water vapor mixing ratio of the inlet air, respectively.

If the outlet air is saturated, then the water vapor mixing ratio of the outlet air from the cooling tower is as follows:

$$e = 6.11 \times 10^{\frac{7.5 \times T_{ao}}{237.3+T_{ao}}} \tag{7}$$

$$d_{ao} = 0.622 \times \frac{e}{P - e} \tag{8}$$

where e denotes the water vapor pressure calculated using the Magnus (1844) empirical formula.

Direct cooling systems (DCS) use sea water to cool the condenser in the buildings (Ho *et al* 2007). If we assume that the sea water volume flow rate, q_{sw}, is constant, then the temperature difference between the inlet and outlet of the system is as follows:

$$\Delta T_{sw} = \frac{H_B^{DCS}}{\rho_{sw} C_{sw} q_{sw}} \tag{9}$$

where ρ_{sw} denotes the sea water density, C_{sw} represents the sea water heat capacity. For the DCS systems in this study, the estimation of the temperature rises of the sea water during one day is around 1×10^{-5} °C, which is ignored in this study.

2.3. Air-conditioning heat partition in BEM

BEM starts from the assumption that the internal target temperature and humidity levels remain within the comfort range (Salamanca *et al* 2010) and then estimates the cooling load inside the buildings. The default air-conditioning system in BEM is the wall-type scenario (shown in figure 2), and is assumed to be used in residential areas in this study. The BEM model calculates the sensible heat fluxes, H_i^{out}, and latent heat fluxes, LE_i^{out}, for each floor, i, into the atmosphere required to maintain standard indoor comfort conditions (Krpo *et al* 2010). The details of the sensible and latent heat flux calculation can be found in Salamanca *et al* (2010). Then, the sensible and latent heat fluxes generated at each floor, i, and released into the

atmosphere through the air-conditioning systems (Krpo *et al* 2010) can be expressed as follows:

$$H_i = \frac{\mathrm{COP}+1}{\mathrm{COP}} H_i^{\mathrm{out}} \tag{10}$$

$$\mathrm{LE}_i = \mathrm{LE}_i^{\mathrm{out}} \tag{11}$$

where COP denotes the coefficient of performance for the air-conditioning systems, which is assumed to be constant for all wall-type systems.

The Baseline case (figure 2) assumes that the systems are settled at the rooftop level. Then, the sensible and latent heat fluxes generated at each floor, *i*, are summed up and released into the atmosphere only at the rooftop level through the air-conditioning systems (followed by Krpo *et al* 2010); these fluxes can be expressed as follows:

$$H_T^{\mathrm{Base}} = \sum_{i=1}^{m} H_i \tag{12}$$

$$\mathrm{LE}_T^{\mathrm{Base}} = \sum_{i=1}^{m} \mathrm{LE}_i. \tag{13}$$

The sensible or latent heat fluxes at the rooftop are given by the sum of turbulent fluxes H_{tur} or $\mathrm{LE}_{\mathrm{tur}}$, from the roof surfaces, which is computed using the Louis formulation (Martilli *et al* 2002) and H_T^{Base} or $\mathrm{LE}_T^{\mathrm{Base}}$, followed by the method proposed by Krpo *et al* (2010).

For the DCS case (figure 2), the sensible heat fluxes generated at each floor, *i*, are summed up and go back to the sea water through DCS systems, which is assumed to be located in the equipment unit in the building (ASHRAE Handbook 2008); this can be expressed as follows:

$$H_B^{\mathrm{DCS}} = \sum_{i=1}^{m} H_i \tag{14}$$

$$\mathrm{LE}_B^{\mathrm{DCS}} = \sum_{i=1}^{m} \mathrm{LE}_i. \tag{15}$$

For the CPCT case (figure 2), the sensible, H_T^{CPCT}, and latent heat fluxes, LE_T^{CPCT}, to the atmosphere at the rooftop level are shown below:

$$H_T^{\mathrm{CPCT}} = m_a C_p \left(T_{\mathrm{ao}} - T_{\mathrm{ai}}\right) \tag{16}$$

$$\mathrm{LE}_T^{\mathrm{CPCT}} = m_a \left(h_{\mathrm{ao}} - h_{\mathrm{ai}}\right) + \sum_{i=1}^{m} \mathrm{LE}_i - H_T^{\mathrm{CPCT}}. \tag{17}$$

Note that for the residential areas, wall-type systems are kept unchanged for all the cases.

3. Results

3.1. Model evaluation

To validate the performance of the Baseline model, the simulation results are compared with surface level observations. The model could reasonably reproduce the physical characteristics of the temperature and wind field distribution (shown in figures 3, 4 and S1 available at stacks.iop.org/ERL/13/034015/mmedia). Figure 3 shows that there are some convergence zones (Tong *et al* 2005) formed at 2:00 pm on 25 June in different areas in Hong Kong. The temperature distribution is basically captured, although the model underestimated the air temperature at some stations, like SEK on 24 (shown in figure S1) and 25 June, which may due to the uncertainty of soil conditions and also the 1° NCEP FNL data chosen as the boundary condition (Takane and Kusaka 2011). The Baseline model could well capture the high temperature area in the convergence zone in Kowloon Peninsula at 3:00 pm on 24 June (figure S1), which is dominated by a westerly sea breeze and easterly wind and 2:00 pm on 25 June (figure 3), which is dominated by a southeastern wind. The observed and simulated 2 m air temperature for all urban and rural sites are compared (shown in figure 4). Note that because the horizontal spatial resolution is limited to 0.5 km, the stations along the coast (CCH, WGL, PEN, and SLW, as shown in figure 1(*d*)) are excluded because they may represent sea surface characteristics due to the land cover and land use classification. The Baseline model could capture the spatial distribution of 2 m air temperature well. The agreement between the Baseline model and observations was set in accordance with the criteria value of mean bias error (MBE), root-mean-square error (RMSE), and index of agreement (IOA) for 2 m air temperature for 27 available stations, which are 0.224, 1.242 and 0.90 respectively. The MBE value between the Baseline model and observations for the urban areas for 2 m air temperature is −0.09 °C. The Baseline model could capture the wind rotation from southwestern to southeastern on 24 June well, particularly in the central area of the Kowloon Peninsula, as shown in figure 5. The model underestimated the wind field when the extreme high-temperature event ended on 28 June, as shown in figure 5. In the Baseline case, the anthropogenic heat releases at the rooftop level and can affect the street level by vertical diffusion (Martilli *et al* 2002, Salamanca *et al* 2010), which is not significant in a high-rise city. In general, the Baseline case could capture the temperature distribution and wind rotation in the urban areas well, which can fulfill the goal of this study.

3.2. Effects of air-conditioning systems on air temperature, humidity, and surface energy balance

To evaluate the contribution of air-conditioning systems on temperature and humidity levels, the 2 m air temperature and the water vapor mixing ratio are chosen as the criteria for comparison. Figure S2 shows the 2 m air temperature distribution at 2:00 pm on June 25, 2016, i.e. the time when the maximum air temperature was recorded, and the temperature difference between the Baseline case and different air-conditioning

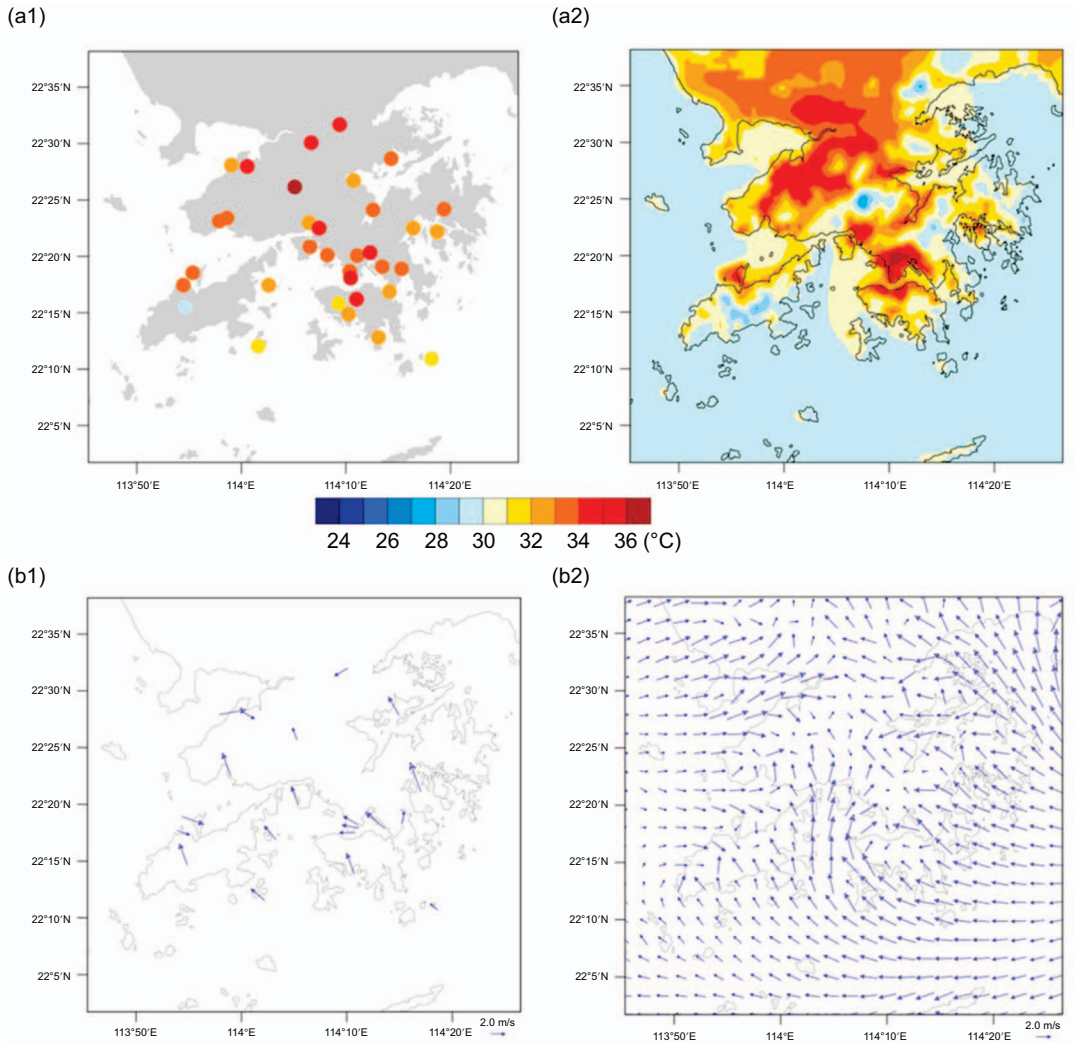

Figure 3. Comparison results of 2 m air temperature at 2:00 pm local time on June 25, 2016, for (*a1*) observation results and (*a2*) Baseline case; and 10 m wind fields for (*b1*) observation values, and (*b2*) Baseline case.

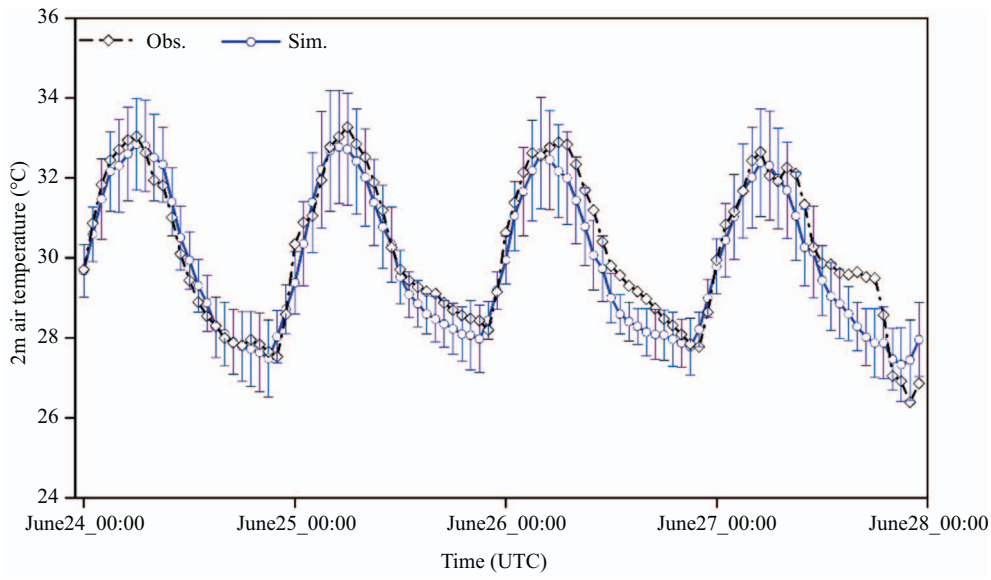

Figure 4. Comparison of observed and simulated 2 m air temperature from 00:00 24 June to 00:00 28 June, 2017.

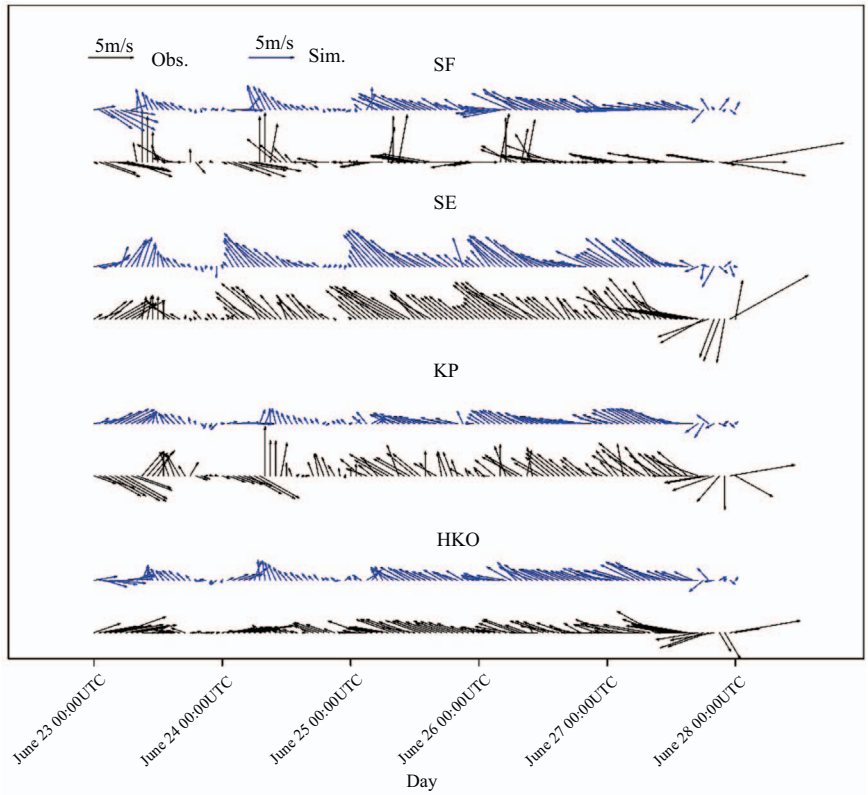

Figure 5. Comparison of observed and simulated surface wind fields at HKO, KP, SE and SF stations. The locations of the four stations are shown in figure 1(*d*).

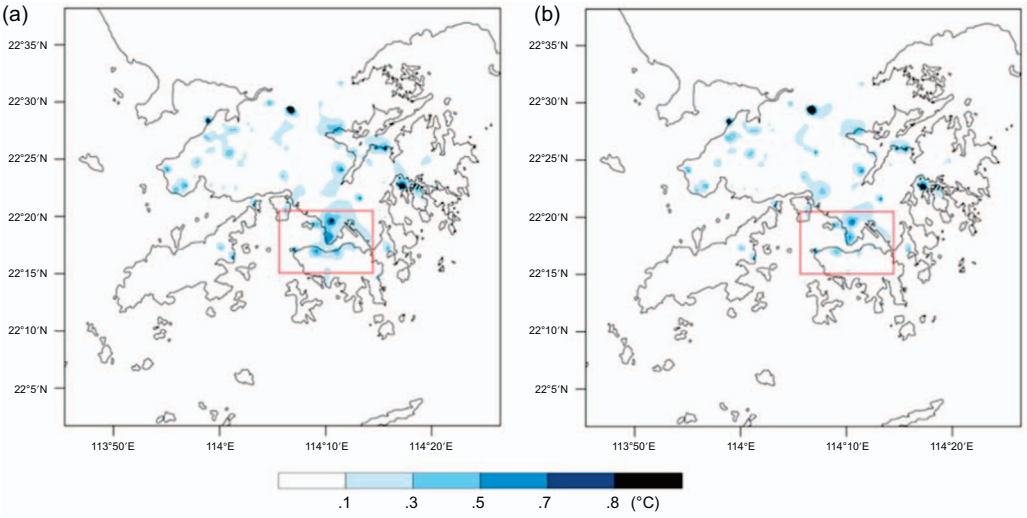

Figure 6. (*a*) Modeled mean 2 m air temperature differences (Baseline case–DCS case) averaged for June 24–28, 2016, from 8:00 am to 8:00 pm. (*b*) Same as (*a*) but for the Baseline case–CPCT case. The rectangular areas in (*a*) and (*b*) denote the areas that have been illustrated in figures 5 and 6.

scenarios at the corresponding time. The use of alternative water-cooled air-conditioning systems could decrease the 2 m air temperature during an extreme high temperature event by around 0.4 °C–0.8 °C, particularly along the northern part of Hong Kong Island and the commercial areas in Kowloon Peninsula, where most high-rise buildings and the high-density population are located. The population density data used in this study are downloaded from Columbia University's Socioeconomic Data and Applications Center. The results also revealed the mean 2 m air temperature differences (figure 6), which were around 0.3 °C–0.8 °C, between the Baseline case and the corresponding air-conditioning scenarios averaged for all the extreme high temperature events from 8:00 am–8:00 pm, when the air-conditioning was switched

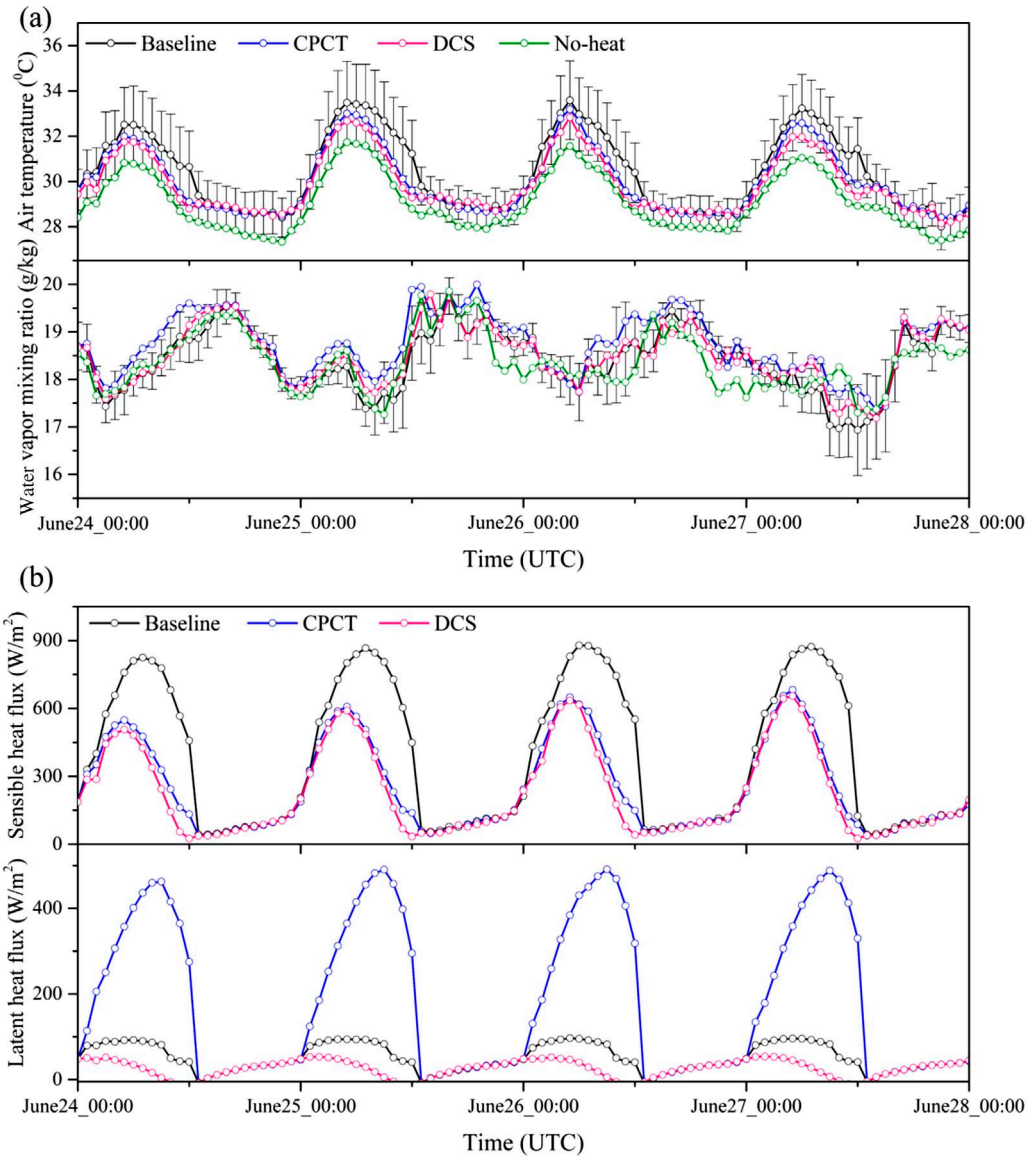

Figure 7. (*a*) Comparison of mean 2 m air temperature and water vapor mixing ratio in non-domestic areas in the specific areas illustrated in figure 4 for the Baseline case, CPCT case, DCS case, and no-heat case; (*b*) similar to (*a*) but for mean sensible and latent heat fluxes. Note here that the vertical bars in (*a*) denote the standard deviation of the air temperature and the water vapor mixing ratio for the Baseline case.

on. The results are in agreement with the findings of other studies (He *et al* 2007, Salamanca *et al* 2014). Further, the large depth evolution of the PBL height during the daytime inhibited the effects of air-conditioning on the urban air temperature as compared to the relatively shallow PBL height and stable atmospheric conditions during the night. If the anthropogenic heat were excluded in the urban areas, the temperature difference could have reached around 4 °C in the commercial areas in Kowloon Peninsula, which was also verified by Wang *et al* (2017). As the non-domestic buildings are mostly concentrated in Kowloon Peninsula and the northern part of Hong Kong Island, an area, marked by the red rectangle in figure 6, is chosen for further investigation. The averaged 2 m air temperature, water vapor mixing ratio, sensible heat fluxes, and latent heat fluxes are compared among the different scenarios (figure 7). The use of water-cooled air systems can reduce the 2 m air temperature by around 0.5 °C–0.8 °C during the daytime as shown in figure 6(*a*), and the DCS case presents around 0.1 °C–0.15 °C lower air temperature as compared to the CPCT case. The temperature differences between the Baseline and the alternative systems reach 1.5 °C at 7:00–8:00 pm, as the impact of air-conditioning systems is more significant during the night-time (Fan and Sailor 2005). The use of cooling tower systems in commercial areas can significantly increase the water vapor mixing ratio in the atmosphere by around 0.29 g kg^{-1} on average. However, an increase in the water mixing ratio in the air will result in an increase in the apparent temperature and the heat index level, which will in turn increase energy consumption to remove the humidity in the supply air (Steadman 1984, Gutiérrez *et al* 2015). The cooling tower diminishes the sensible heat by around

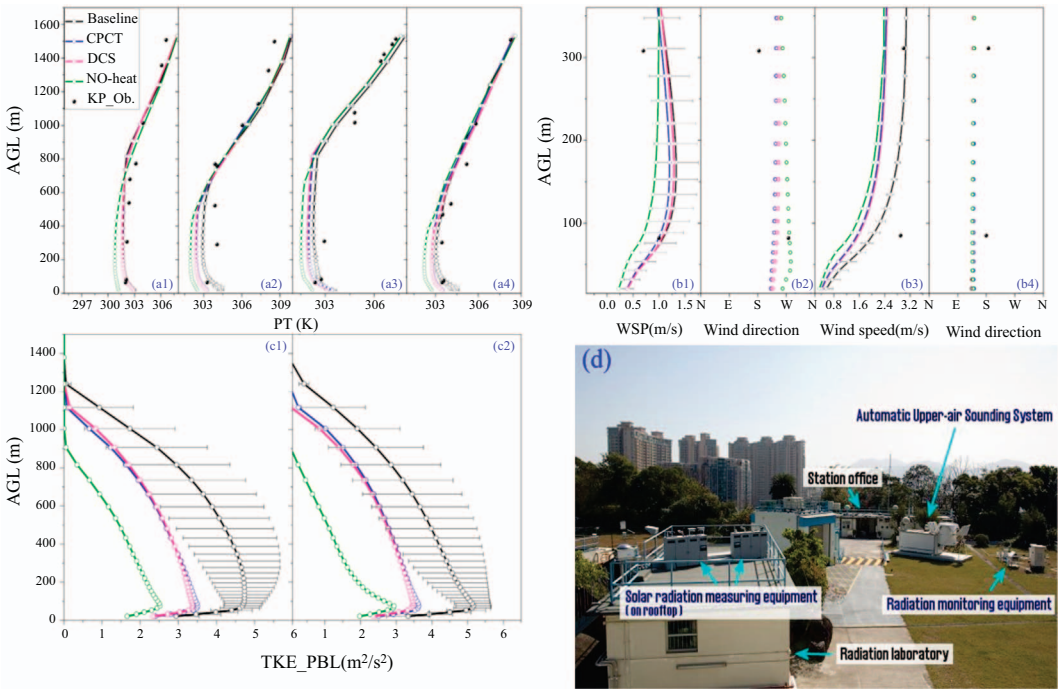

Figure 8. Comparison of mean potential temperature (K) in the nine grid points near King's Park station for the Baseline case, CPCT case, DCS case, and no-heat case, and the observation value at (*a1*) 00:00 UTC and (*a2*) 12:00 UTC on June 24, and (*a3*) 00:00 UTC and (*a4*) 12:00 UTC on June 25, 2016; similar to (*a1*)–(*a4*) but for mean wind speed and wind direction at (*b1*, *b2*) 00:00 UTC and (*b3*) and (*b4*) 12:00 UTC on June 24, 2016; similar to (*a1*)–(*a4*) but for mean TKE_PBL at 06:00 UTC on (*c1*) June 24, and (*c2*) June 25, 2016; (*d*) shows the layout and the instruments of King's Park Meteorological Station. Note here that the horizontal bars denote the standard deviation of specific parameters (source: www.hko.gov.hk).

80%–90% and transforms it into latent heat flux (Milosavljevic and Heikkilä 2001) during the afternoon with the maximum value delayed for around 1–2 as compared to the maximum sensible heat fluxes for the Baseline case, as shown in figure 7(*b*). As sensible heat fluxes are the sum of H_{tur} and H_T^{Base} (Krpo *et al* 2010), the differences between the Baseline case and the CPCT and DCS cases with respect to the sensible heat fluxes indicate the heat fluxes from the air-conditioning systems (figure 7(*b*)). The sensible heat fluxes in the CPCT case are slightly higher than those in the DCS case, while in the CPCT case, the latent heat fluxes contribute almost 90% of the energy emitted by the air-conditioning systems (figure 7(*b*)). Ichinose *et al* (1999) reported that the anthropogenic heat emission in central Tokyo exceeds 400 W m^{-2} in the daytime, and the maximum value could be 1590 W m^{-2}. The anthropogenic heat flux in Hong Kong using satellite data was studied by Wong *et al* (2015), and the results show that commercial areas emit the largest anthropogenic heat fluxes around 500–600 W m^{-2} compared with other land-use types. The use of different air-conditioning systems affects the surface energy balance, and air-cooled air systems (Baseline case) could significantly increase sensible heat fluxes through the air-conditioning systems and enhanced turbulence fluxes.

3.3. Effects on vertical structures

The effects of city-scale air-conditioning systems on vertical structures were investigated. The use of different air-conditioning systems could not only modify the surface energy balance but also extended to the areas above the ground level, which affects the development of the PBL height (Fan and Sailor 2005, Chen *et al* 2009, Sailor 2011, Gutiérrez *et al* 2015), as shown in figure S3. The PBL height presents diurnal variation, with the peak value of around 1400 m to 1600 m occurring at around 13:00–14:00 pm and around 500–600 m during the night (shown in figure S3). The implementation of the two alternative air-conditioning systems modifies the heat emitted and generation of turbulence, which induces a 100–150 m reduction in the PBL height. A reduction of the PBL height could cause potential air pollution issues (Han *et al* 2009, Gutiérrez *et al* 2015).

The Baseline case has a relatively high urban canopy temperature, as shown in figures 8(*a1*)–(*a4*) on the vertical potential temperature, which leads to thermal discomfort for pedestrians and high building energy consumption (Nikolopoulou *et al* 2001, Salamanca *et al* 2010). The vertical profile of the potential temperature (figure 8) shows a higher value below 300 m in the Baseline case than in the other cases at the same height, which illustrates that anthropogenic heat from the air-conditioning systems enhances vertical mixing (Salamanca *et al* 2014). Differences in the potential temperature between the different cases are reduced with an increase in height (figures 8(*a1*)–(*a4*)), which shows the effect of anthropogenic heat fluxes on the potential temperature distribution at the lower level (Chen *et al* 2009).

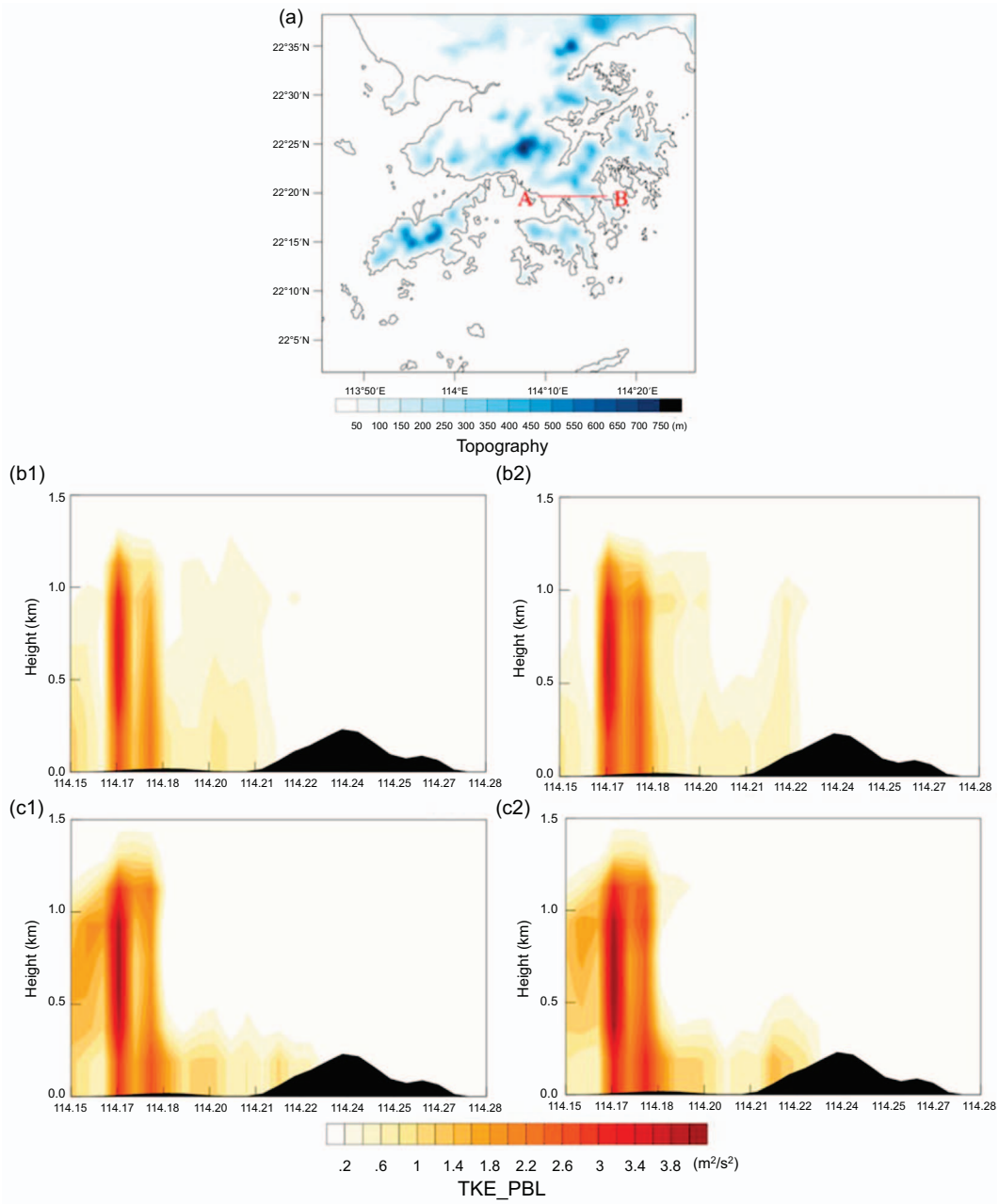

Figure 9. Vertical east–west cross-section (transect A–B, shown in (*a*)) of the difference in TKE_PBL ($m^2\ s^{-2}$) above ground level up to 1.5 km at 06:00 UTC on (*b1*, referring to the Baseline–CPCT case) and (*b2*, referring to the Baseline–DCS case) June 24, 2016, and at 06:00 UTC on (*c1*, referring to the Baseline–CPCT case) and (*c2*, referring to the Baseline–DCS case) June 25, 2016.

The momentum fluxes for the horizontal surfaces are determined by the bulk Richardson number based on Louis formulation, which is a function of roof roughness length, wind speed and the air temperature (Martilli *et al* 2002). The differences in the potential temperature affect the wind speed, and the Baseline case has the largest horizontal wind velocity (figures 8(*b1*)–(*b4*)). Figures 8(*b1*)–(*b4*) further illustrate that the wind direction is not affected by the different schemes of air-conditioning systems.

The selection of an air-conditioning system affects the sensible heat fluxes released into the atmosphere, as discussed in section 2.2, which has a direct effect on the buoyant production of turbulent kinetic energy (TKE) (Martilli *et al* 2002). The results show that the buoyant production of TKE has the largest magnitude for the Baseline case and the smallest for the no-heat case (figures 8(*c1*)–(*c2*)). The largest differences in TKE were found 100 m above the ground level, above the mean building height of the region. Furthermore, figure 9 shows that the differences in the buoyant TKE are extended to a height of around 1.3 km above the ground level in the commercial areas, which has no influence in the non-domestic areas. The decreases in TKE within the urban boundary layer lead to potential air pollution issues, particularly pollutants near the ground level (Chen *et al* 2009, Salamanca *et al* 2010, Sharma *et al* 2016).

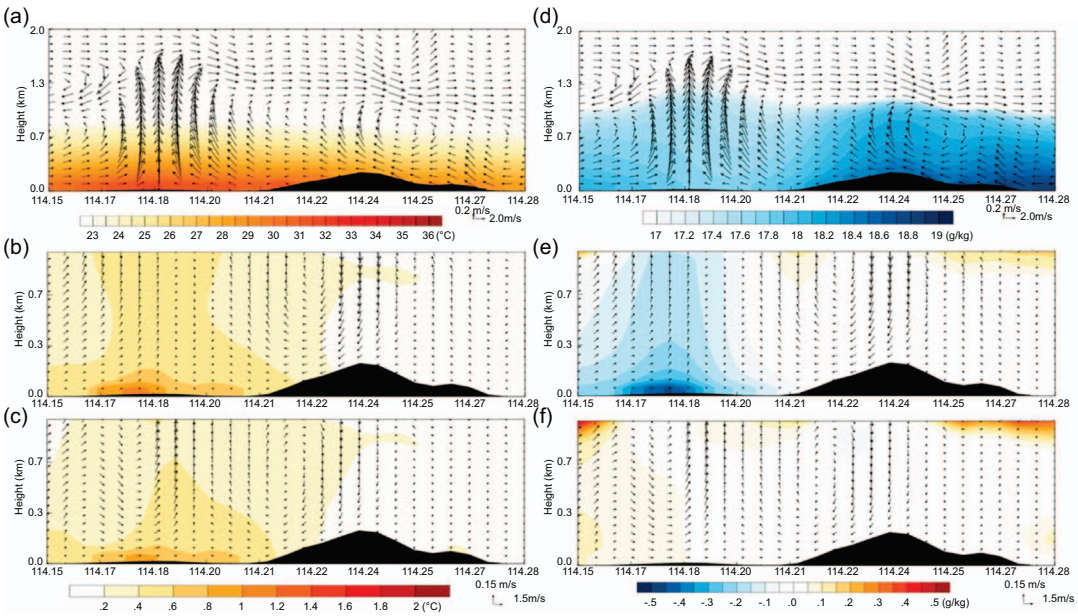

Figure 10. Vertical east–west cross-section (transect A–B, shown in figure 7(*a*)) at 06:00 UTC on June 24, 2016, of (*a*) simulated wind fields (m s^{-1}) (vectors) and temperature (°C) (shaded) above ground level up to 2.0 km for the Baseline Case; (*b*) difference in wind fields (m s^{-1}) (vectors) and temperature (°C) (shaded) above ground level up to 1.0 km (referring to the Baseline–CPCT case); (*c*) similar to (*b*) but for the Baseline–DCS case; (*d*) simulated wind fields (m s^{-1}) (vectors) and water vapor mixing ratio (g kg^{-1}) (shaded) for the Baseline case; (*e*) difference in wind fields (m s^{-1}) (vectors) and water vapor mixing ratio (g kg^{-1}) (shaded) above ground level up to 1.0 km (referring to the Baseline–CPCT case); and (*f*) similar to (*e*) but for the Baseline–DCS case.

3.4. Effects on SLBC and UHIC

The effect of different air-conditioning systems on local wind circulation, particularly UHIC and SLBC, is investigated in the urban areas (vertical East–West cross-section, transect A–B, shown in figure 9(*a*)) in Kowloon Peninsula. At 06:00 UTC on 24 June 2016, a convergence zone was observed in the urban areas of Kowloon Peninsula (Tong *et al* 2005), with sea breeze penetration on the left side and a downslope wind on the right side. The urban areas in the convergence zone area are characterized by a low water vapor mixing ratio and enhanced UHIC of up to around 1.5 km (as shown in figures 10(*a*) and (*d*)). On the right side of the convergence zone, the UHIC is stronger than on the left side with the assistance of the airflow from across the mountain (as shown in figure 10(*a*)). Across the mountain, the water vapor mixing ratio is also reduced (figure 10(*a*)). To further investigate the effects of different air-conditioning scenarios on the local circulation, the difference in vertical wind fields is examined. The CPCT case has a higher water vapor mixing ratio near the ground level in the urban areas (on the left side of the convergence zone, shown in figure 10(*e*)), which is in agreement with Gutiérrez *et al* (2015). Figures 10(*b*) and (*c*) show that the Baseline case has the largest sensible heat fluxes and can enhance the downslope wind on the mountain side merged into the UHI circulation. The DCS case has less sensible and latent heat fluxes, which leads to a large vertical velocity difference, as shown in figure 10(*c*). Both cases (figures 10(*b*) and (*c*)) show a decrease in the vertical velocity in the urban areas, particularly in the convergence zone areas, which could reduce the strength of the UHIC (Chen *et al* 2009, Chen *et al* 2011, Xie *et al* 2016). Changing to the alternative air-conditioning systems could reduce the near-ground air temperature by around 0.4 °C–0.8 °C (figures 10(*b*) and (*c*)) for both cases, which in turn reduces the strength of the sea breeze.

At 06:00 UTC on 25 June 2016, the background wind was southeasterly, and the urban areas in the cross-section were dominated by a strong eastern wind and no sea breeze penetration (figure S4(*a*)). The urban areas were characterized by a low water vapor mixing ratio as well. The largest vertical wind velocity was near the western edge of the cross-section, and the UHIC moved west in comparison to that shown in figure 10(*a*). The Baseline case, with the largest sensible heat fluxes within the urban canopy layer, had a strong UHIC. The changes in air-conditioning systems could not only affect the vertical distribution of the air temperature and the water vapor mixing ratio, but also the secondary local circulation, particularly the sea breeze circulation and the UHI circulation.

4. Discussion

The Baseline case has a higher air temperature within the urban canopy layer than the CPCT and DCS cases, which implies that the alternative systems can enhance pedestrian thermal comfort from this aspect. However, the CPCT and DCS cases show a decrease in sensible heat fluxes (figure 7), horizontal and vertical wind speed (figure 8), buoyant production of TKE

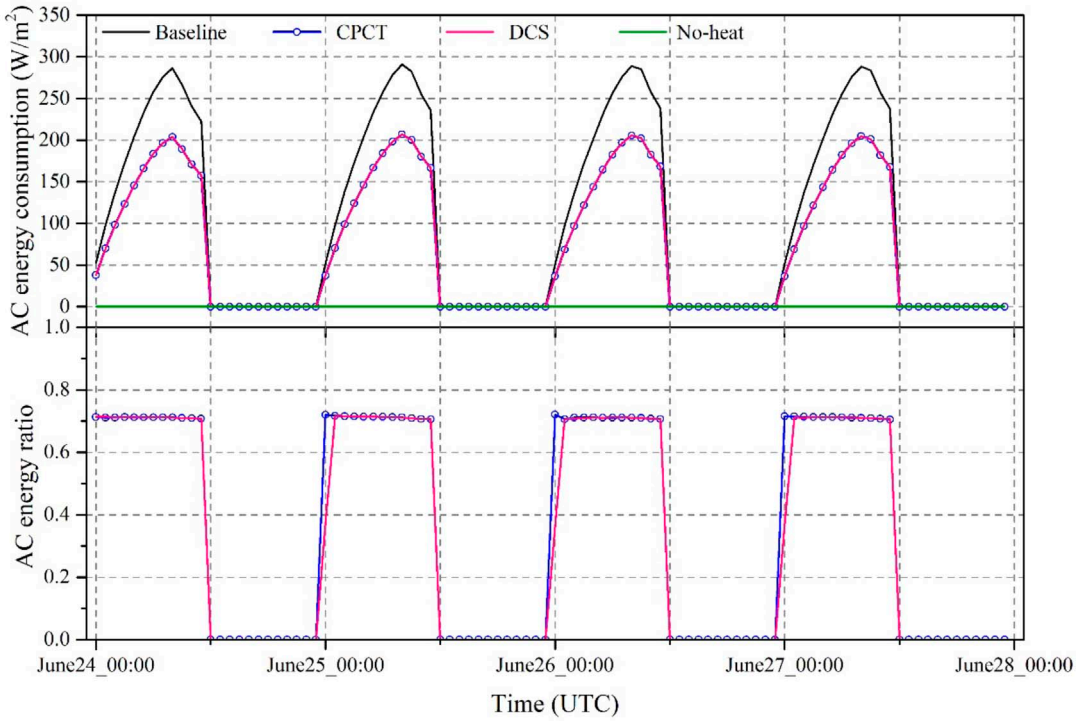

Figure 11. Comparison of air-conditioning energy consumption in the non-domestic areas in the specific areas shown in figure 4 for the Baseline case, CPCT case, DCS case, and no-heat case (upper), and the energy saving ratio for the CPCT and DCS cases as compared to that in the Baseline case (below).

(figures 8 and 9), and PBL height (figure S3). The air-conditioning systems also affect secondary circulation, SLBC, and UHIC. The changes may cause air stagnation and air pollution issues near the ground level, particularly in the convergence areas in Kowloon Peninsula (Tong *et al* 2005, Chen *et al* 2009, Salamanca *et al* 2010, Xie *et al* 2016). Xie *et al* (2016) clearly showed that the changes in the meteorological conditions due to the anthropogenic heat fluxes can significantly affect the spatial and vertical distributions of air pollutants, particularly in the big cities in China. The role of sea land breeze circulation on the coastal and inland areas has been investigated (Kitada 1987, Melas *et al* 1995, Clappier *et al* 2000). An increase in the pollutant level usually combines with a relatively weak sea breeze and unfavorable conditions for pollutant dispersion (Papanastasiou and Melas 2009). Therefore, the hypothesis for air quality issues needs to be confirmed in the future.

The energy consumption using different air-conditioning systems is investigated, and in this study, the COP for the Wall_type, Baseline, CPCT, and DCS cases are set as 2.0, 2.5, 3.5, and 3.5, respectively, on the basis of the findings of other studies (Ashie *et al* 1999, Ho *et al* 2007, Salamanca *et al* 2010, Huang *et al* 2013). Figure 11 shows the averaged air-conditioning fluxes in the non-domestic areas (as shown in figure 6) and the energy saving with the alternative air-conditioning systems referring to the Baseline case. The results clearly show that in the CPCT and DCS cases, the energy consumption of the air-conditioning systems was effectively reduced, with 30% energy savings in comparison to that in the Baseline case. Note that here, the cost of changing the systems and maintenance is not considered. In making the decision to choose alternative systems, one must consider the competing benefits and disadvantages.

5. Conclusions

This study is a step forward in investigating the effects of two alternative air-conditioning systems (DCS and CPCT) on urban climate according to the real-life conditions of Hong Kong. The two air-conditioning systems are physically based, parameterized, implemented in the WRF model coupled with the BEP-BEM urban canopy model, and assessed during an extreme high temperature event at the city scale of Hong Kong. Note that the performance of the alternative air-conditioning systems under different climatic scenarios is beyond the scope of this study but will be studied in the future.

The results show that both water-cooled air systems could reduce the 2 m air temperature by around 0.5 °C–0.8 °C during the daytime, and the temperature differences between the Baseline and the two alternative systems could reach 1.5 °C at 7:00 pm–8:00 pm when the PBL height was confined to 100 m. The sensible heat fluxes in the CPCT case were slightly higher than in the DCS case, while in the CPCT case, the latent heat fluxes contributed almost 90% of the energy

emission from the air-conditioning systems. The cooling tower (CPCT case) diminished around 80%–90% of the sensible heat fluxes and transformed them into latent heat fluxes, which could significantly increase the water vapor mixing ratio in the atmosphere by around 0.29 g kg^{-1} on average.

Environmental and meteorological effects are not confined to the rooftop where the air-conditioning systems are located, but can extend to the surface and alter the vertical distribution of various parameters within the urban boundary layer. The implementation of the two alternative air-conditioning systems modified the heat and turbulence, which affected the evolution of the PBL height (with a reduction in height of 100–150 m), and also reduced vertical mixing. Moreover, the CPCT and DCS cases exhibited lower horizontal wind speed and buoyant production of TKE, which might cause air pollution issues, particularly near the ground level. Hence, the hypothesis on the air quality issue needs to be confirmed in the future. The alternative air-conditioning systems could affect the secondary local circulation, which reduces the strength of the SLBC and UHIC in the urban areas.

Certain aspects of energy consumption were illustrated, and the CPCT and DCS cases could effectively reduce the air-conditioning energy consumption by 30% as compared to the Baseline case. The non-extreme high temperature period (June 8–9, 2016) showed that water-cooled air systems could reduce the 2 m air temperature by around 0.6 °C–1.0 °C in the commercial areas, which was higher than in the June 23–28, 2016, period, and had similar effects on the boundary dynamics. The new results from this study are expected to help define UHI mitigation strategies. However, installation and maintenance costs are not considered. In making the decision to choose alternative systems, one must consider the competing benefits and disadvantages.

Acknowledgments

This work is supported financially by an RGC CRF project (HKU9/CRF/12G) of the Hong Kong SAR Government. The weather data for individual stations were obtained through collaboration with Hong Kong Observatory. The input and output data used in this study are available for academic research upon request from the corresponding author.

ORCID iDs

Y Wang https://orcid.org/0000-0002-9406-9732

References

Allen L, Lindberg F and Grimmond C S B 2011 Global to city scale urban anthropogenic heat flux: model and variability *Int. J. Climatol.* **31** 1990–2005

Ashie Y, Ca V T and Asaeda T 1999 Building canopy model for the analysis of urban climate *J. Wind Eng. Ind. Aerodyn.* **81** 237–48

ASHRAE Handbook 2008 *HVAC Systems and Equipment* (Atlanta: American Society of Heating, Refrigerating and Air Conditioning Engineers) p 33

Bonacquisti V, Casale G R, Palmieri S and Siani A M 2006 A canopy layer model and its application to Rome *Sci. Total Environ.* **364** 1–13

Bougeault P and Lacarrere P 1989 Parameterization of orography-induced turbulence in a mesobeta-scale model *Mon. Weather Rev.* **117** 1872–90

Chen C, Hu G and Kang L 2014 Key technology study on thermal balance of ground source heat pump in territories with a cold winter and a warm summer *Int. Conf. IEA Heat Pump*

Chen F and Dudhia J 2001 Coupling an advanced land surface—hydrology model with the Penn State—NCAR MM5 modeling system. Part I: model implementation and sensitivity *Mon. Weather Rev.* **129** 569–85

Chen F, Miao S, Tewari M, Bao J W and Kusaka H 2011 A numerical study of interactions between surface forcing and sea breeze circulations and their effects on stagnation in the greater Houston area *J. Geophys. Res. Atmos.* **116** D12105

Chen F *et al* 2011 The integrated WRF/urban modelling system: development, evaluation, and applications to urban environmental problems *Int. J. Climatol.* **31** 273–88

Chen F, Yang X and Zhu W 2014 WRF simulations of urban heat island under hot-weather synoptic conditions: the case study of Hangzhou City, China *Atmos. Res.* **138** 364–77

Chen Y, Jiang W M, Zhang N, He X F and Zhou R W 2009 Numerical simulation of the anthropogenic heat effect on urban boundary layer structure *Theor. Appl. Climatol.* **97** 123–34

Clappier A, Martilli A, Grossi P, Thunis P, Pasi F, Krueger B C, Calpini B, Graziani G and van den Bergh H 2000 Effect of sea breeze on air pollution in the greater Athens area. Part I: numerical simulations and field observations *J. Appl. Meteorol.* **39** 546–62

De Bono A, Peduzzi P, Kluser S and Giuliani G 2004 Impacts of summer 2003 heat wave in Europe *Environ. Alert Bull.* **2** 1–4

de Munck C, Pigeon G, Masson V, Meunier F, Bousquet P, Tréméac B, Merchat M, Poeuf P and Marchadier C 2013 How much can air conditioning increase air temperatures for a city like Paris, France *Int. J. Climatol.* **33** 210–27

Dudhia J 1989 Numerical study of convection observed during the winter monsoon experiment using a mesoscale two-dimensional model *J. Atmos. Sci.* **46** 3077–107

Fan H and Sailor D J 2005 Modeling the impacts of anthropogenic heating on the urban climate of Philadelphia: a comparison of implementations in two PBL schemes *Atmos. Environ.* **39** 73–84

Feng J M, Wang Y L, Ma Z G and Liu Y H 2012 Simulating the regional impacts of urbanization and anthropogenic heat release on climate across China *J. Clim.* **25** 7187–203

Flanner M G 2009 Integrating anthropogenic heat flux with global climate models *Geophys. Res. Lett.* **36** L02801

Grimmond C S B 1992 The suburban energy balance: Methodological considerations and results for a mid-latitude west coast city under winter and spring conditions *Int. J. Climatol.* **12** 481–97

Gutiérrez E, González J E, Martilli A and Bornstein R 2015 On the anthropogenic heat fluxes using an air conditioning evaporative cooling parameterization for mesoscale urban canopy models *J. Sol. Energy Eng.* **137** 051005

Han S, Bian H, Tie X, Xie Y, Sun M and Liu A 2009 Impact of nocturnal planetary boundary layer on urban air pollutants: measurements from a 250 m tower over Tianjin, China *J. Hazard Mater.* **162** 264–69

He X F, Jiang W M, Chen Y and Liu G 2007 Numerical simulation of the impacts of anthropogenic heat on the structure of the urban boundary layer *Chinese J. Geophys.* **50** 75–83

Ho S K, Tam L S and Lo S K 2007 Adoption of water-cooled air conditioning systems for territory-wide energy improvement *Int. Conf. Climate Change*

Hong S Y, Dudhia J and Chen S H 2004 A revised approach to ice microphysical processes for the bulk parameterization of clouds and precipitation *Mon. Weather Rev.* **132** 103–20

Huang Y, Niu J L and Chung T M 2013 Study on performance of energy-efficient retrofitting measures on commercial building external walls in cooling-dominant cities *Appl. Energy* **103** 97–108

Ichinose T, Shimodozono K and Hanaki K 1999 Impact of anthropogenic heat on urban climate in Tokyo *Atmos. Environ.* **33** 3897–909

Kain J S and Fritsch J M 1990 A one-dimensional entraining/detraining plume model and its application in convective parameterization *J. Atmos. Sci.* **47** 2784–802

Kikegawa Y, Genchi Y, Yoshikado H and Kondo H 2003 Development of a numerical simulation system toward comprehensive assessments of urban warming countermeasures including their impacts upon the urban buildings' energy-demands *Appl. Energy* **76** 449–66

Kitada T 1987 Turbulence structure of sea breeze front and its implication in air pollution transport-application of k-ϵ turbulence model *Bound. Layer Meteorol.* **41** 217–39

Krpo A, Salamanca F, Martilli A and Clappier A 2010 On the impact of anthropogenic heat fluxes on the urban boundary layer: a two-dimensional numerical study *Bound. Layer Meteorol.* **136** 105–27

Ma S, Pitman A, Hart M, Evans J P, Haghdadi N and MacGill I 2017 The impact of an urban canopy and anthropogenic heat fluxes on Sydney's climate *Int. J. Climatol.* **37** 255–70

Magnus G 1844 *Versuche über die Spannkräfte des Wasserdampfs Annalen der Physik* **137** 225–47

Mansur E T, Mendelsohn R and Morrison W 2008 Climate change adaptation: a study of fuel choice and consumption in the US energy sector *J. Environ. Econ. Manage.* **55** 175–93

Martilli A, Clappier A and Rotach M W 2002 An urban surface exchange parameterisation for mesoscale models *Bound. Layer Meteorol.* **104** 261–304

Melas D, Kambezidis H D, Walmsley J L, Moussiopoulos N, Bornstein R D, Klemm O, Asimakopoulos D N and Schiermeier F A 1995 NATO/CCMS Pilot study workshop on air pollution trarfsport and diffusion over coastal urban areas *Atmos. Environ.* **29** 3713–8

Milosavljevic N and Heikkilä P 2001 A comprehensive approach to cooling tower design *Appl. Therm. Eng.* **21** 899–915

Mlawer E J, Taubman S J, Brown P D, Iacono M J and Clough S A 1997 Radiative transfer for inhomogeneous atmospheres: RRTM, a validated correlated-k model for the longwave *J. Geophys. Res. Atmos.* **102** 16663–82

Nikolopoulou M, Baker N and Steemers K 2001 Thermal comfort in outdoor urban spaces: understanding the human parameter *Sol. Energy* **70** 227–35

Ohashi Y, Genchi Y, Kondo H, Kikegawa Y, Yoshikado H and Hirano Y 2007 Influence of air-conditioning waste heat on air temperature in Tokyo during summer: numerical experiments using an urban canopy model coupled with a building energy model *J. Appl. Meteorol. Climatol.* **46** 66–81

Oke T R 1976 The distinction between canopy and boundary-layer urban heat islands *Atmosphere* **14** 268–77

Oke T R 1987 *Boundary Layer Climates* 2nd edn (York: Methuen) p 289

Oke T R 1988 The urban energy balance *Prog. Phys. Geogr.* **12** 471–508

Papanastasiou D K and Melas D 2009 Climatology and impact on air quality of sea breeze in an urban coastal environment *Int. J. Climatol.* **29** 305–15

Pigeon G, Legain D, Durand P and Masson V 2007 Anthropogenic heat release in an old European agglomeration (Toulouse, France) *Int. J. Climatol.* **27** 1969–81

Quah A K and Roth M 2012 Diurnal and weekly variation of anthropogenic heat emissions in a tropical city, Singapore *Atmos. Environ.* **46** 92–103

Sailor D J and Lu L 2004 A top-down methodology for developing diurnal and seasonal anthropogenic heating profiles for urban areas *Atmos. Environ.* **38** 2737–48

Sailor D J 2011 A review of methods for estimating anthropogenic heat and moisture emissions in the urban environment *Int. J. Climatol.* **31** 189–99

Salamanca F, Krpo A, Martilli A and Clappier A 2010 A new building energy model coupled with an urban canopy parameterization for urban climate simulations-part I. formulation, verification, and sensitivity analysis of the model *Theor. Appl. Climatol.* **99** 331

Salamanca F, Martilli A, Tewari M and Chen F 2011 A study of the urban boundary layer using different urban parameterizations and high-resolution urban canopy parameters with WRF *J. Appl. Meteorol. Climatol.* **50** 1107–28

Salamanca F, Martilli A and Yagüe C 2012 A numerical study of the Urban Heat Island over Madrid during the DESIREX 2008 campaign with WRF and an evaluation of simple mitigation strategies *Int. J. Climatol.* **32** 2372–86

Salamanca F, Georgescu M, Mahalov A, Moustaoui M and Wang M 2014 Anthropogenic heating of the urban environment due to air conditioning *J. Geophys. Res. Atmos.* **119** 5949–65

Sharma A, Conry P, Fernando H J S, Hamlet A F, Hellmann J J and Chen F 2016 Green and cool roofs to mitigate Urban Heat Island effects in the Chicago metropolitan area: evaluation with a regional climate model *Environ. Res. Lett.* **11** 64004

Skamarock W C, Klemp J B, Dudhia J, Gill D O, Barke D, Duda M G, Huang X Y and Wang W 2008 *NCAR Technical Note* NCAR/TN-475+STR p 113

Steadman R G 1984 A universal scale of apparent temperature *J. Clim. Appl. Meteorol.* **23** 1674–87

Taha H 1997 Urban climates and heat Islands: albedo, evapotranspiration, and anthropogenic heat *Energy Build.* **25** 99–103

Takane Y and Kusaka H 2011 Formation mechanisms of the extreme high surface air temperature of 40.9 °C observed in the Tokyo metropolitan area: considerations of dynamic foehn and foehnlike wind *J. Appl. Meteorol. Climatol.* **50** 1827–41

Tong H, Walton A, Sang J and Chan J C 2005 Numerical simulation of the urban boundary layer over the complex terrain of Hong Kong *Atmos. Environ.* **39** 3549–63

US Energy Information Administration 2012 Annual Energy Review 2011 *Technical Report* No. DOE/EIA-0384

Wang Y, Di Sabatino S, Martilli A, Li Y, Wong M S, Gutiérrez E and Chan P W 2017 Impact of land surface heterogeneity on urban heat island circulation and sea-land breeze circulation in Hong Kong *J. Geophys. Res. Atmos.* **122** 4332–52

Wen Y and Lian Z 2009 Influence of air conditioners utilization on urban thermal environment *Appl. Therm. Eng.* **29** 670–5

Wong M S, Yang J, Nichol J, Weng Q, Menenti M and Chan P W 2015 Modeling of anthropogenic heat flux using HJ-1 B Chinese small satellite image: a study of heterogeneous urbanized areas in Hong Kong *IEEE Geosci Remote S.* **12** 1466–70

Xie M, Liao J, Wang T, Zhu K, Zhuang B, Han Y, Li M and Li S 2016 Modeling of the anthropogenic heat flux and its effect on regional meteorology and air quality over the Yangtze River Delta region, China *Atmos. Chem. Phys.* **16** 6071–89

Yang W, Chen B and Cui X 2014 High-resolution mapping of anthropogenic heat in China from 1992–2010 *Int. J. Environ. Res. Public Health* **11** 4066–77

Zampieri M, Russo S, di Sabatino S, Michetti M, Scoccimarro E and Gualdi S 2016 Global assessment of heat wave magnitudes from 1901–2010 and implications for the river discharge of the Alps *Sci. Total Environ.* **571** 1330–9